

UV and IR Spectroscopic Studies of Cold Alkali Metal Ion–Crown Ether Complexes in the Gas Phase

**Yoshiya Inokuchi,^{‡,*} Oleg V. Boyarkin,[†] Ryoji Kusaka,[‡] Takeharu Haino,[‡]
Takayuki Ebata[‡] and Thomas R. Rizzo^{†,*}**

*Department of Chemistry, Graduate School of Science, Hiroshima University,
Higashi-Hiroshima, Hiroshima 739-8526, Japan and Laboratoire de Chimie Physique
Moléculaire, École Polytechnique Fédérale de Lausanne, Lausanne CH-1015,
Switzerland*

Abstract

We report UV photodissociation (UVPD) and IR-UV double-resonance spectra of dibenzo-18-crown-6 (DB18C6) complexes with alkali metal ions (Li^+ , Na^+ , K^+ , Rb^+ , and Cs^+) in a cold, 22-pole ion trap. All the complexes show a number of vibronically resolved UV bands in the 36000–38000 cm^{-1} region. The Li^+ and Na^+ complexes each exhibit two stable conformations in the cold ion trap (as verified by IR-UV double-resonance), whereas the K^+ , Rb^+ , and Cs^+ complexes exist in a single conformation. We analyze the structure of the conformers with the aid of density functional theory (DFT) calculations. In the Li^+ and Na^+ complexes, DB18C6 distorts the ether ring to fit the cavity size to the small diameter of Li^+ and Na^+ . In the complexes with K^+ , Rb^+ , and Cs^+ , DB18C6 adopts a boat-type (C_{2v}) open conformation. The K^+ ion is captured in the cavity of the open conformer thanks to the optimum

matching between the cavity size and the ion diameter. The Rb^+ and Cs^+ ions sit on top of the ether ring, because they are too large to enter the cavity of the open conformer. According to time-dependent DFT calculations, complexes that are highly distorted to hold metal ions open the ether ring upon S_1 - S_0 excitation, and this is confirmed by extensive low-frequency progressions in the UVPD spectra.

*To whom correspondence should be addressed. E-mail:
y-inokuchi@hiroshima-u.ac.jp (YI), thomas.rizzo@epfl.ch (TRR).

‡Hiroshima University

†École Polytechnique Fédérale de Lausanne

in the gas phase with mass spectrometric techniques,⁴⁻¹⁶ ion mobility methods,^{17,18} and more recently by IR spectroscopy.¹⁹⁻²⁵ The structure of benzo-crown ethers and their complexes with neutral guest species was studied by UV and IR spectroscopy under jet-cooled conditions.²⁶⁻³² Very recently, Kim and coworkers reported UV spectra of metal ion–DB18C6 complexes produced by electrospray.³³⁻³⁵ Although they cooled the complexes to 150 K in the gas phase, the UV spectra still showed only broad features.

In the present work, we return to the original method of Pedersen for studying cation–DB18C6 complexes, UV spectroscopy, but we combine it with cooling in an ion trap.^{36,37} We report here UV photodissociation (UVPD) spectra of DB18C6 complexes with alkali metal ions, $M^+\bullet$ DB18C6 ($M = \text{Li, Na, K, Rb, and Cs}$). The $M^+\bullet$ DB18C6 complexes are produced by nanoelectrospray, mass-selected by a quadrupole mass spectrometer and irradiated with a UV laser in a cold, 22-pole ion trap, where the complexes are cooled down to ~ 10 K.^{36,37} Isolating and cooling the complexes in the gas phase greatly simplify the UV spectra and provide well-resolved vibronic bands. Furthermore, we measure conformer-specific infrared spectra *via* IR-UV double-resonance in the CH stretching ($2800\text{--}3120\text{ cm}^{-1}$) region. Although the observed IR spectra are more congested than predicted by quantum chemical calculations because of Fermi resonance interactions, we can still use these spectra to distinguish peaks in the UV spectra that belong to different conformers. The use of density functional theory (DFT) allows us to determine the conformation of the complexes.

2. Experimental and computational methods

The details of our experimental approach have been given elsewhere.³⁸

Briefly, $M^+ \cdot \text{DB18C6}$ ($M = \text{Li, Na, K, Rb, and Cs}$) complexes are produced continuously at atmospheric pressure *via* nanoelectrospray using 20–200 μM solutions of DB18C6 and metal chloride salts in methanol. Ions are transferred into a vacuum chamber through an 11.5 cm long stainless steel capillary and injected into an ion funnel, which is used for collecting and focusing the divergent stream of ions exiting the capillary. After leaving the funnel, the ions pass through a hexapole ion guide and a quadrupole mass filter before being deflected 90° by an electrostatic quadrupole and stored in a room temperature octopole ion trap. The trap accumulates the continuous stream of ions and ejects them in packets with a repetition rate of 10 Hz. The resulting ion packets are deflected by a second electrostatic quadrupole before entering a 22-pole RF ion trap, which is housed in a copper box and cooled by a closed cycle He refrigerator to 4 K. The trapped ions are cooled internally and translationally to low temperature through collisions with cold He buffer gas, which is injected into the trap volume using a pulsed valve. The vibrational temperature of ions is estimated to be ~ 10 K.^{36,37} The trapped ions are then irradiated with a UV laser pulse, which causes some fraction of them to dissociate. The resulting charged photofragments, as well as the remaining parent ions, are released from the trap, deflected 90° by a third quadrupole deflector, mass-analyzed by a quadrupole mass filter and detected with a channel electron multiplier. Ultraviolet photodissociation spectra of parent ions are obtained by plotting the yield of a particular photofragment ion as a function of the wavenumber of the UV laser. The UV light comes from the frequency-doubled output of a dye laser, which is pumped with the third harmonic of a Nd:YAG laser. For IR-UV double-resonance spectroscopy, we use a tunable IR optical parametric oscillator (OPO) pumped with a Nd:YAG laser. The output pulse of the IR OPO counter-propagates collinearly with the UV pulse, arriving in the trap ~ 100 ns prior to it. The

wavenumber of the UV laser is fixed to a particular vibronic band in the UVPD spectra for monitoring the population of the zero-point level of a conformer. The wavenumber of the OPO is scanned while monitoring fragment ion intensity induced by the UV laser. Conformer-specific IR spectra are obtained by plotting the yield of a particular photofragment as a function of the OPO wavenumber. For distinguishing vibronic bands due to different conformers, we measure UVPD spectra with the OPO wavenumber fixed to a particular vibrational band. The detailed procedure of IR-UV double-resonance spectroscopy is described in the Supporting Information.

For geometry optimization of the DB18C6 complexes with alkali metal ions, we first use a classical force field to find conformational minima. The initial conformational search is performed by using the mixed torsional search with low-mode sampling and the MMFF94s force field as implemented in MacroModel V. 9.1.³⁹ Within a 41.84 kJ/mol (10.00 kcal/mol) energy window, 219, 201, 123, 109, and 83 conformations are found for the Li⁺, Na⁺, K⁺, Rb⁺, and Cs⁺ complexes, respectively. Minimum-energy conformers found with the force field calculations are then optimized at the M05-2X/6-31+G(d) level with *loose* optimization criteria with the GAUSSIAN09 program package.⁴⁰ Unique minima obtained by comparison of relative energies (tolerance 0.05 kJ/mol) and rotational constants are further optimized at the M05-2X/6-31+G(d) and wB97XD/6-31++G(d,p) levels. Vibrational analysis is carried out for the optimized structures at the same level of calculation. The oscillator strength and transition energy of electronic transitions are obtained with time-dependent DFT (TD-DFT) at the M05-2X/6-31+G(d) level. In addition, geometry optimization in the S₁ state is also performed with TD-DFT at the M05-2X/6-31+G(d) level; the optimized structures in the S₀ state are used as the starting point for optimization of the

excited state structures. For Rb and Cs, we use several effective core potentials (ECPs) such as LanL2DZ, Stuttgart RLC, Stuttgart RSC 1997, and CRENL; functions of these ECPs are obtained from a database of basis sets.⁴¹ For comparison with the calculated results of Choi et al.,³⁴ we also calculate all the complexes using the B3LYP functional. All the experimental and calculated results and their analysis are described in the Supporting Information. We use the character “S” for referring to figures in the Supporting Information, e.g. “Fig. 1S”.

3. Results

3.1. UV spectroscopy

Figure 1 displays the UVPD spectra of (a) room temperature $\text{K}^+\cdot\text{DB18C6}$ and (b) $\text{K}^+\cdot\text{DB18C6}$ that is cooled in the 22-pole ion trap. The uncooled complex has a broad absorption around 36300 cm^{-1} , which is similar to the UVPD spectrum measured at 150 K.³⁴ The UV spectrum of the cooled $\text{K}^+\cdot\text{DB18C6}$ complex consists of many sharp bands, with the band origin clearly observed at 36415 cm^{-1} . From the intensity and the vibrational frequency of hot bands observed on the low energy side of the band origin, we estimate the temperature of the cooled complex to be $\sim 10\text{ K}$. Comparison of the UV spectra in Fig. 1 indicates that the broad absorption of the uncooled complex is mainly due to thermal congestion.

Figure 2 shows the UVPD spectra of the cooled $\text{M}^+\cdot\text{DB18C6}$ ($\text{M} = \text{Li}, \text{Na}, \text{K}, \text{Rb}, \text{and Cs}$) complexes in the $35500\text{--}38000\text{ cm}^{-1}$ region together with the LIF spectrum of bare, jet-cooled DB18C6.²⁸ Except for the Li^+ complex, these UVPD spectra are measured by monitoring the yield of the M^+ photofragment ions. The Li^+ ion ($m/Z = 7$) could not be detected with the second quadrupole mass filter because of its low-mass cutoff. However upon UV excitation the $\text{Li}^+\cdot\text{DB18C6}$ complex produces a variety of

photofragments that result from the decomposition of the ether ring, as shown in Fig. 1S. The spectrum in Fig. 2a is measured by detecting the photofragment cation at $m/Z = 309$, which corresponds to the loss of $\text{CH}_2\text{-OCH}_2\text{CH}_2$. All the $\text{M}^+\cdot\text{DB18C6}$ complexes show a blue shift of the absorption relative to uncomplexed DB18C6. In UV spectroscopic studies of $\text{DB18C6-(H}_2\text{O)}_n$ complexes, the attachment of H_2O molecules to the α oxygen atoms (O1, O4, O10, and O13, see Scheme 1) through the $\text{O-H}\cdots\text{O}$ hydrogen bond causes a blue-shift of the $\text{S}_1\text{-S}_0$ absorption.^{28,29} This suggests that the metal ions in the $\text{M}^+\cdot\text{DB18C6}$ complexes are bonded to the α oxygen atoms, and the shift in the band origin in the UVPD spectra is an indication of the interaction strength. The Li^+ complex shows the most blue-shifted band origin, indicating the strongest interaction. This result is consistent with enthalpies of binding measured by collision-induced dissociation.¹⁶ For the Rb^+ and Cs^+ complexes, the band origin gradually shifts to the red with respect to the position of the K^+ complex. This indicates that the interaction between the α oxygen atoms and the metal ion becomes progressively weaker from K^+ to Cs^+ .

Figure 3 displays expanded views of the UVPD spectra of the $\text{K}^+\cdot\text{DB18C6}$, $\text{Rb}^+\cdot\text{DB18C6}$, and $\text{Cs}^+\cdot\text{DB18C6}$ complexes around their respective band origins. In the previous study, the UV spectra of the K^+ , Rb^+ , and Cs^+ complexes exhibited only broad features.³⁴ In contrast, the cold UV spectra of Fig. 3 exhibit many resolved features that provide a rich source of information on the complexes. As is highlighted by solid lines, the spectral features exhibit a band splitting of a few cm^{-1} . Based on the study of UV spectroscopy for jet-cooled DB18C6, we assign this structure to the exciton splitting that occurs between the benzene rings.²⁸ The doublet structure appears repeatedly in the spectra, built on top of vibrational progressions of ~ 20 and 47

cm^{-1} , which are due to low-frequency vibrations of the complexes (labeled α and β in Fig. 3). In addition, the spectra have weak features assignable to hot bands. Superscript and subscript integers with α and β denote quantum numbers of these vibrations in the S_1 and S_0 states, respectively. The progression starts not only from the origin band (0_0^0) but from a hot band (α_1^0). As seen in Fig. 2 or Fig. 8S, the vibronic pattern around the origin band appears also in the higher frequency region. These patterns are due to vibrations involving mainly the benzene rings, and the frequency is almost the same for the K^+ , Rb^+ , and Cs^+ complexes. The interval of the exciton splitting and vibrational frequencies are collected in Table 1.

3.2. IR spectroscopy

All the UVPD spectra in Fig. 2 have a number of vibronically resolved bands. In order to distinguish vibronic bands due to different conformers, IR-UV double-resonance spectra are measured using strong vibronic bands. Figure 4 shows the IR-UV spectra of the $\text{M}^+\cdot\text{DB18C6}$ complexes in the CH stretching ($2800\text{--}3120\text{ cm}^{-1}$) region. For the Li^+ and Na^+ complexes, two kinds of IR spectra are found; the IR-UV spectra in Figs. 4a–d are measured by monitoring the intensity of the vibronic bands labeled Li-I, Li-II, Na-I, and Na-II in Fig. 2. These results indicate that there exist at least two conformers for the Li^+ and Na^+ complexes. The IR-UV spectra of the K^+ , Rb^+ , and Cs^+ complexes in Figs. 4e–g are observed by monitoring the origin band (K-I, Rb-I, and Cs-I in Fig. 2). Using other vibronic bands of these complexes produces the same IR spectra, demonstrating that there is only one stable isomer for each of them. The similarity of the IR spectra of the K^+ , Rb^+ , and Cs^+ complexes imply that the conformation of DB18C6 in each of them will be similar. We also perform hole-burning experiments with the IR laser in order to confirm the number of

conformers. UVPD spectra of the $M^+\cdot\text{DB18C6}$ complexes are measured under the IR irradiation with the wavenumber fixed to a particular vibrational band. With these UV measurements we distinguish which peaks in the UVPD spectra belong to different conformers (see Figs. 3S and 4S). If different conformers have a similar IR absorption spectrum, it is difficult to distinguish them with IR spectroscopy. Therefore, the number of conformers determined in this study is a lower limit. Nevertheless, we have carefully measured IR spectra for most of strong vibronic bands in the UVPD spectra, and all the IR spectra can be classified into one of the spectra in Fig. 4. On this basis we can say that if any other conformers exist under the cold conditions of our ion trap they represent at best a minor fraction of the total complex population.

After sorting the vibronic bands by conformers, we can analyze the vibronic structure in the UVPD spectra more definitively, as described in detail in the Supporting Information. For the Li^+ complex, the origin band of the two stable conformers is strong, one of which is accompanied by an extensive low-frequency progression with an interval of 19.1 cm^{-1} (see Fig. 5S). For the Na^+ complex, the origin band is too weak to be identified, and low-frequency progressions are extensive for both of the stable conformers (see Fig. 6S). As seen in Fig. 3, low-frequency progressions can be seen also for the K^+ , Rb^+ , and Cs^+ complexes, but these are not so extensive. We discuss more fully below the relation between the activity of the low-frequency progressions in the UV spectra and the conformation of the complexes.

4. Discussion

4.1. Determination of the conformation for the $M^+\cdot\text{DB18C6}$ complexes

We determine the structure of the $M^+\cdot\text{DB18C6}$ complexes with the aid of

DFT and TD-DFT. For the Li^+ and Na^+ complexes, the two conformers identified in the UVPD spectra can be attributed to the most and the second most stable forms calculated at the M05-2X level, because these are substantially more stable than others. (The calculated total energy for all the conformers is described in the Supporting Information.) Figure 5 displays the lowest-energy structures of the $\text{Li}^+\cdot\text{DB18C6}$ and $\text{Na}^+\cdot\text{DB18C6}$ complexes calculated at the M05-2X/6-31+G(d) level. In the previous study by Choi et al., the $\text{Li}^+\cdot\text{DB18C6}$ complex was ascribed to another structure (Li-c in Fig. 9S) on the basis of B3LYP calculations.³⁴ However, the possibility of the structure (Li-c) as the conformation of $\text{Li}^+\cdot\text{DB18C6}$ is ruled out by the absence of the exciton splitting in the UVPD spectrum, as described in the Supporting Information.

Calculated structures of the K^+ , Rb^+ , and Cs^+ complexes are shown in Fig. 6. The K^+ complex has a boat-type C_{2v} conformer (K-a in Fig. 6a). This is the most stable conformer at all the levels of B3LYP/6-31+G(d), M05-2X/6-31+G(d), and wB97XD/6-31++G(d,p). From the similarities among the UVPD spectra and the IR-UV spectra, we expect the Rb^+ and Cs^+ complexes to have a C_{2v} structure similar to K-a. However, the predominance of the boat C_{2v} conformers (Rb-a and Cs-b in Fig. 6) is not so clear from the calculations of the Rb^+ and Cs^+ complexes. For the Rb^+ complex, all the calculations show that the boat conformation (Rb-a) is the most stable form, but there is another conformer (Rb-b in Fig. 12S) with a total energy very close to that of Rb-a. In the case of the Cs^+ complex, the boat C_{2v} conformer (Cs-b) is the second most stable form at the M05-2X and wB97XD calculations; the most stable one (Cs-a in Fig. 13S) has a structure similar to Rb-b. The stabilization energy is dependent on the DFT functionals and the ECPs used in geometry optimization. Therefore, the structure of the Rb^+ and Cs^+ complexes cannot be determined definitely

on the basis of their calculated energy. As shown in Fig. 23S, the observed IR spectra are more congested than predicted by the DFT calculations, which is due to the Fermi resonance interactions between the CH stretching and overtone of the CH bending vibrations. Therefore, comparison of the observed and calculated IR spectra does not provide a definitive conclusion for the complex structure.

In contrast, the assignment of the structure is confirmed with TD-DFT calculations, which do not strongly depend on the calculation methods. Figure 7 shows electronic spectra calculated with TD-DFT at the M05-2X/6-31+G(d) level. For the calculated electronic transition energies, a scaling factor of 0.8340 is used for comparison with the experimental spectra. This factor is determined so as to reproduce the transition energy of the origin band of the $\text{K}^+\cdot\text{DB18C6}$ complex with the most stable conformer (K-a). The transition energy calculated for Rb-a (C_{2v}) and Cs-b (C_{2v}) is coincident with the position of the origin bands for the Rb^+ and Cs^+ complexes, while Rb-b and Cs-a show band origins that are blue-shifted with respect to that of K-a rather than red-shifted (as observed). These results reinforce the assignment of the structure of the Rb^+ and Cs^+ complexes to Rb-a and Cs-b. In the case of the Li^+ and Na^+ complexes, the second most stable conformers (Li-b and Na-b) show electronic transition energies lower than those of the most stable ones (Li-a and Na-a). Therefore, we attribute the vibronic bands of Li-I and Li-II to conformers Li-b and Li-a, respectively. Similarly, Na-I and Na-II in the UVPD spectrum are ascribed to Na-b and Na-a, respectively. In both Li-a and Li-b, DB18C6 distorts its ether ring to hold the Li^+ ion, because the cavity size of DB18C6 is much larger than Li^+ . This distortion is also seen also for Na-a and Na-b. However, the distance between the oxygen atoms and the Na^+ ion is longer (2.39 Å) than that of Li-a and Li-b (2.09 Å), and the ether ring

is not so highly distorted as in the Li^+ complex. In K-a, Rb-a, and Cs-b, the ether ring of DB18C6 opens the most, adopting a boat (C_{2v}) conformation. The K^+ ion is in the center of the cavity, while the Rb^+ and Cs^+ ions sit on top of the open cavity because their ion diameters are larger than the cavity size. The conformer structures in Figs. 5 and 6 are similar to those predicted by Bowers and coworkers on the basis of ion mobility measurements for alkali complexes with B18C6.^{17,18}

We can compare the gas-phase structures in Figs. 5 and 6 with those obtained by X-ray diffraction analysis of alkali metal salts with DB18C6. The Cambridge Structural Database (CSD ver. 5.31) of the Cambridge Crystallographic Data Centre⁴² contains 32, 59, 10, and 3 crystal structures for the Na^+ , K^+ , Rb^+ , and Cs^+ complexes, respectively. No crystal data of the $\text{Li}^+\cdot\text{DB18C6}$ complex was put into the database. Rb^+ and Cs^+ ions are each held by two DB18C6 molecules in all the crystals, implying that they are too large to be located inside the DB18C6 cavity. For all the K^+ complexes in crystals, the DB18C6 part has a boat-type open form, similar to that in the gas phase (Fig. 6a).^{43,44} In contrast, the $\text{Na}^+\cdot\text{DB18C6}$ complex in crystals has structures quite different from that in the gas phase.⁴⁵⁻⁴⁸ In crystals the conformation of the DB18C6 adopts an open form, similar to that in the $\text{K}^+\cdot\text{DB18C6}$ complex, whereas the ether ring is distorted in the gas phase to fitting the cavity size to Na^+ (Figs. 5c and 5d). In crystals, counterions also take part in the coordination of metal cations, which significantly influences the complex structure. Since alkali metal complexes of DB18C6 are separated from counter anions in solution, the structure of the complexes in solution should be more similar to that in the gas phase than in crystals.

4.2. Conformation change upon UV irradiation

Activity of low-frequency vibrational progressions in a UV spectrum is an

indication of a structural change along the vibrational coordinates of low-frequency normal modes upon S_1 - S_0 excitation. Geometry optimization in the S_1 and S_0 states well explains the activity of the progressions observed in the UVPD spectra of the complexes we have measured. Vibrational analysis in the S_0 state shows that all the conformers in Figs. 5 and 6 have low-frequency vibrations of $\sim 20\text{ cm}^{-1}$, which are torsional motions of the ether ring. Based on these results, the low-frequency progressions observed in the UVPD spectra can be attributed to torsional motions of the ring in the S_1 state. As shown in Fig. 7S, the torsional motions involve a change of the distance between the benzene rings. Therefore, the distance can be used as a measure of the structural change upon S_1 - S_0 excitation. Table 2 shows the distance between the benzene rings in the S_0 and S_1 state and the difference in the distance for the conformers in Figs. 5 and 6. Li-b, Na-a, and Na-b show much larger differences ($\sim 0.45\text{ \AA}$) than those of Li-a, K-a, Rb-a, and Cs-b ($\sim 0.10\text{ \AA}$). These calculated results coincide well with the experimental observations in that one of the Li^+ conformers and both of the Na^+ conformers show the extensive and intense low-frequency vibrational progressions, as seen in Figs. 5S and 6S. All the conformers in Table 2 show an increase of the distance between the benzene rings from the S_0 to S_1 states. The conformers in which the distance in the S_0 state is shorter than $\sim 7.80\text{ \AA}$ tend to have larger structural change, which causes the extensive low-frequency progressions in the UVPD spectra. This indicates that complexes that are highly distorted open the ether ring more extensively upon S_1 - S_0 excitation, especially in the cases of Li^+ and Na^+ . As a result, the metal ions will be exposed more on the outside of the ether ring, which may change their chemical activity. This suggests that the encapsulation of metal ions in the cavity of DB18C6 could perhaps be controlled by UV irradiation.

5. Summary

We have measured UV photodissociation (UVPD) and IR-UV double-resonance spectra of the $M^+\cdot\text{DB18C6}$ ($M = \text{Li, Na, K, Rb, and Cs}$) complexes produced by nanoelectrospray and cooled to ~ 10 K in the 22-pole ion trap. All the $M^+\cdot\text{DB18C6}$ complexes show a number of well-resolved vibronic bands. With the aid of quantum chemical calculations, we conclude the following: (1) The $\text{Li}^+\cdot\text{DB18C6}$ and $\text{Na}^+\cdot\text{DB18C6}$ complexes exhibit two stable conformers in our cold ion trap, whereas the K^+ , Rb^+ , and Cs^+ complexes show only one. (2) For holding Li^+ or Na^+ , DB18C6 distorts the ether ring to fit the cavity size to the ion diameter. (3) In the $\text{K}^+\cdot\text{DB18C6}$ complex, the DB18C6 opens the ether cavity the most, and the K^+ ion fits well inside. (4) For the Rb^+ and Cs^+ complexes, DB18C6 has an open form similar to the $\text{K}^+\cdot\text{DB18C6}$ complex. However, since the ion size is too large to fit inside the cavity of DB18C6, the ion sits on top of the ether ring and the interaction between the α oxygen atoms and the ions becomes weaker than that of the K^+ complex. (5) Complexes that are highly distorted to hold metal ions open the ether ring largely upon S_1-S_0 excitation. As a result, the encapsulation of metal ions in the cavity of DB18C6 could perhaps be controlled by the UV irradiation.

Acknowledgment

This work is supported by Grant-in-Aids (Grant No. 21350016) for Scientific Research from the Ministry of Education, Culture, Sports, Science, and Technology (MEXT) of Japan and the Swiss National Science foundation through grant 200020_130579. TE thanks the support of MEXT for the Scientific Research on Priority Area “Molecular Science for Supra Functional Systems” (No. 477). YI also thanks the support from the Excellent Young Researchers Overseas Visit Program of Japan Society for the Promotion of Science (JSPS).

Supporting Information Available: Results of IR-UV double-resonance spectroscopy, analysis of the vibronic structure in the UVPD spectra, optimized structures, electronic spectra calculated with the TD-DFT calculations, and a full list of authors of Ref. 40. This material is available free of charge *via* the internet at <http://pubs.ac.org>.

References

- ¹ Pedersen, C. J. *J. Am. Chem. Soc.* **1967**, *89*, 7017–7036.
- ² Pedersen, C. J. *Science* **1988**, *241*, 536–540.
- ³ Shizuka, H.; Takada, K.; Morita, T. *J. Phys. Chem.* **1980**, *84*, 994–999.
- ⁴ Zhang, H.; Chu, I.-H.; Leming, S.; Dearden, D. V. *J. Am. Chem. Soc.* **1991**, *113*, 7415–7417.
- ⁵ Zhang, H.; Dearden, D. V. *J. Am. Chem. Soc.* **1992**, *114*, 2754–2755.
- ⁶ Maleknia, S.; Brodbelt, J. *J. Am. Chem. Soc.* **1992**, *114*, 4295–4298.
- ⁷ Chu, I.-H.; Zhang, H.; Dearden, D. V. *J. Am. Chem. Soc.* **1993**, *115*, 5736–5744.
- ⁸ Brodbelt, J. S.; Liou, C.-C. *Pure & Appl. Chem.* **1993**, *65*, 409–414.
- ⁹ Dearden, D. V.; Zhang, H.; Chu, I.-H.; Wong, P.; Chen, Q. *Pure & Appl. Chem.* **1993**, *65*, 423–428.
- ¹⁰ Ray, D.; Feller, D.; More, M. B.; Glendening, E. D.; Armentrout, P. B. *J. Phys. Chem.* **1996**, *100*, 16116–16125.
- ¹¹ Sobott, F.; Kleinekofort, W.; Brutschy, B. *Anal. Chem.* **1997**, *69*, 3587–3594.
- ¹² More, M. B.; Ray, D.; Armentrout, P. B. *J. Phys. Chem. A* **1997**, *101*, 4254–4262.
- ¹³ More, M. B.; Ray, D.; Armentrout, P. B. *J. Phys. Chem. A* **1997**, *101*, 7007–7017.
- ¹⁴ More, M. B.; Ray, D.; Armentrout, P. B. *J. Am. Chem. Soc.* **1999**, *121*, 417–423.
- ¹⁵ Armentrout, P. B. *Int. J. Mass Spectrom.* **1999**, *193*, 227–240.

- ¹⁶ Anderson, J. D.; Paulsen, E. S.; Dearden, D. V. *Int. J. Mass Spectrom.* **2003**, *227*, 63–76.
- ¹⁷ Lee, S.; Wyttenbach, T.; von Helden, G.; Bowers, M. T. *J. Am. Chem. Soc.* **1995**, *117*, 10159–10160.
- ¹⁸ Wyttenbach, T.; von Helden, G.; Bowers, M. T. *Int. J. Mass Spectrom. Ion Proc.* **1997**, *165/166*, 377–390.
- ¹⁹ Rodriguez, J. D.; Vaden, T. D.; Lisy, J. M. *J. Am. Chem. Soc.* **2009**, *131*, 17277–17285.
- ²⁰ Rodriguez, J. D.; Lisy, J. M. *J. Phys. Chem. A* **2009**, *113*, 6462–6467.
- ²¹ Rodriguez, J. D.; Lisy, J. M. *Int. J. Mass Spectrom.* **2009**, *283*, 135–139.
- ²² Rodriguez, J. D.; Kim, D.; Tarakeshwar, P.; Lisy, J. M. *J. Phys. Chem. A* **2010**, *114*, 1514–1520.
- ²³ Martínez-Haya, B.; Hurtado, P.; Hortal, A. R.; Steill, J. D.; Oomens, J.; Merklings, P. *J. Phys. Chem. A* **2009**, *113*, 7748–7752.
- ²⁴ Martínez-Haya, B.; Hurtado, P.; Hortal, A. R.; Hamad, S.; Steill, J. D.; Oomens, J. *J. Phys. Chem. A* **2010**, *114*, 7048–7054.
- ²⁵ Hurtado, P.; Hortal, A. R.; Gámez, F.; Hamad, S.; Martínez-Haya, B. *Phys. Chem. Chem. Phys.* **2010**, *12*, 13752–13758.
- ²⁶ Shubert, V. A.; James III, W. H.; Zwier, T. S. *J. Phys. Chem. A* **2009**, *113*, 8055–8066.

- ²⁷ Shubert, V. A.; Müller, C. W.; Zwier, T. S. *J. Phys. Chem. A* **2009**, *113*, 8067–8079.
- ²⁸ Kusaka, R.; Inokuchi, Y.; Ebata, T. *Phys. Chem. Chem. Phys.* **2007**, *9*, 4452–4459.
- ²⁹ Kusaka, R.; Inokuchi, Y.; Ebata, T. *Phys. Chem. Chem. Phys.* **2008**, *10*, 6238–6244.
- ³⁰ Kusaka, R.; Inokuchi, Y.; Ebata, T. *Phys. Chem. Chem. Phys.* **2009**, *11*, 9132–9140.
- ³¹ Kokubu, S.; Kusaka, R.; Inokuchi, Y.; Haino, T.; Ebata, T. *Phys. Chem. Chem. Phys.* **2010**, *12*, 3559–3565.
- ³² Kusaka, R.; Inokuchi, Y.; Xantheas, S. S.; Ebata, T. *Sensors* **2010**, *10*, 3519–3548.
- ³³ Kim, H. J.; Shin, W. J.; Choi, C. M.; Lee, J. H.; Kim, N. J. *Bull. Korean Chem. Soc.* **2008**, *29*, 1973–1976.
- ³⁴ Choi, C. M.; Kim, H. J.; Lee, J. H.; Shin, W. J.; Yoon, T. O.; Kim, N. J.; Heo, J. *J. Phys. Chem. A* **2009**, *113*, 8343–8350.
- ³⁵ Choi, C. M.; Lee, J. H.; Choi, Y. H.; Kim, H. J.; Kim, N. J.; Heo, J. *J. Phys. Chem. A* **2010**, *114*, 11167–11174.
- ³⁶ Boyarkin, O. V.; Mercier, S. R.; Kamariotis, A.; Rizzo, T. R. *J. Am. Chem. Soc.* **2006**, *128*, 2816–2817.
- ³⁷ Rizzo, T. R.; Stearns, J. A.; Boyarkin, O. V. *Int. Rev. Phys. Chem.* **2009**, *28*, 481–515.

- ³⁸ Svendsen, A.; Lorenz, U. J.; Boyarkin, O. V.; Rizzo, T. R. *Rev. Sci. Instrum.* **2010**, *81*, 073107 (7 pages).
- ³⁹ Mohamadi, F.; Richards, N. G. J.; Guida, W. C.; Liskamp, R.; Lipton, M.; Caufield, C.; Chang, G.; Hendrickson, T.; Still, W. C. *J. Comput. Chem.* **1990**, *11*, 440–467.
- ⁴⁰ Gaussian 09, Revision A.02, Frisch M. J. et al., Gaussian, Inc., Wallingford CT, 2009.
- ⁴¹ Schuchardt, K. L.; Didier, B. T.; Elsethagen, T.; Sun, L.; Gurumoorthi, V.; Chase, J.; Li, J.; Windus, T. L. *J. Chem. Inf. Model.* **2007**, *47*, 1045–1052.
- ⁴² Allen F. H. *Acta Cryst.* **2002**, *B58*, 380–388.
- ⁴³ Poonia, N. S.; Truter, M. R. *J. Chem. Soc. Dalton Trans.* **1973**, 2062–2065.
- ⁴⁴ Bianchi, A.; Giusti, J.; Paoletti, P.; Mangani, S. *Inorg. Chim. Acta* **1986**, *117*, 157–164.
- ⁴⁵ Bright, D.; Truter, M. R. *Nature* **1970**, *225*, 176–177.
- ⁴⁶ Bright, D.; Truter, M. R. *J. Chem. Soc. B* **1970**, 1544–1550.
- ⁴⁷ Bush, M. A.; Truter, M. R. *J. Chem. Soc. D* **1970**, 1439–1440.
- ⁴⁸ Bush, M. A.; Truter, M. R. *J. Chem. Soc. B* **1971**, 1440–1446.

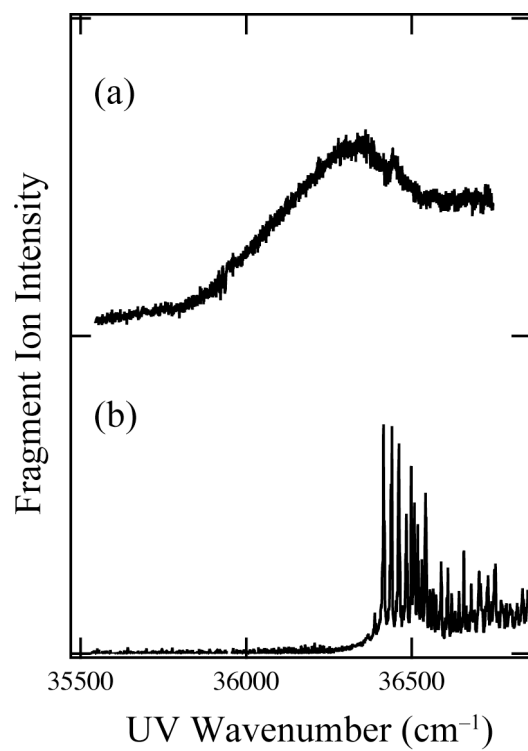


Figure 1. The UVPD spectra of (a) uncooled $\text{K}^+\cdot\text{DB18C6}$ and (b) $\text{K}^+\cdot\text{DB18C6}$ that is cooled in the 22-pole ion trap. The temperature of the cooled complex is estimated to be ~ 10 K.

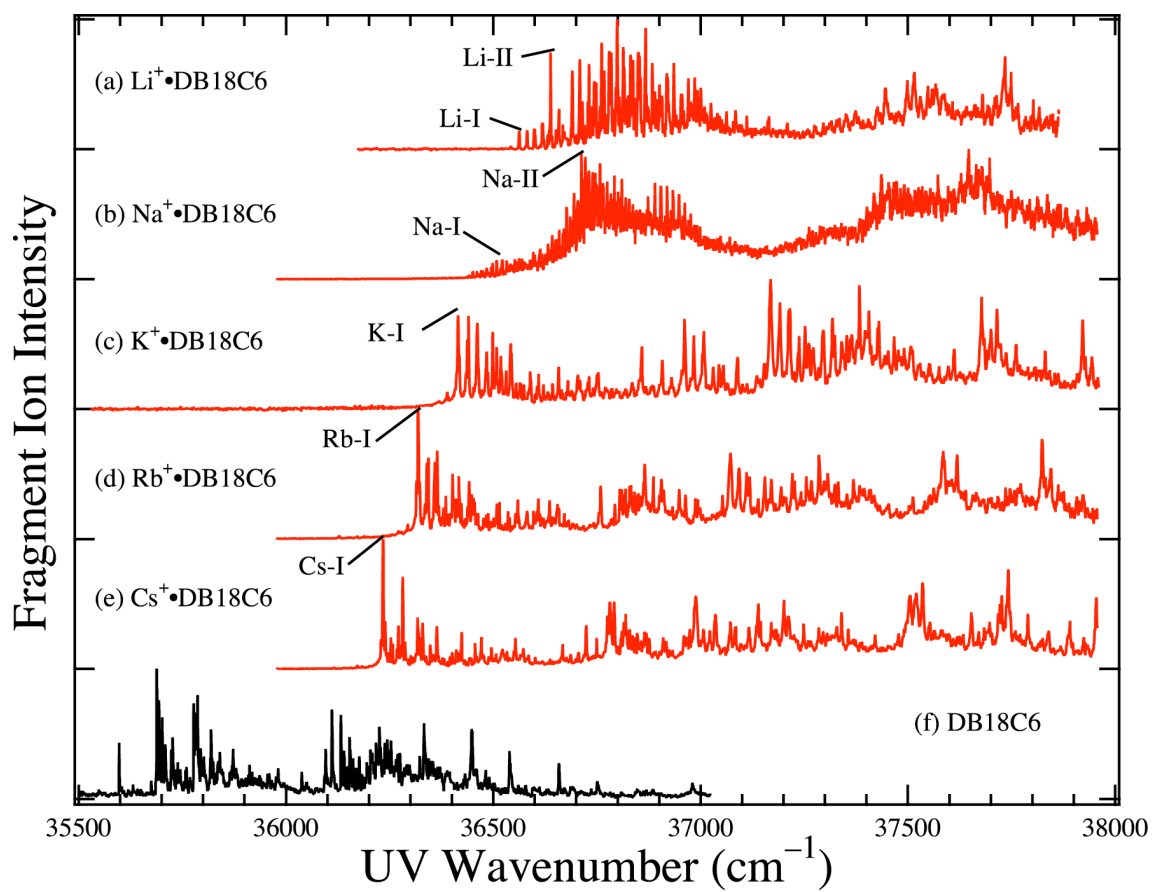


Figure 2. The UVPD spectra of the $M^+\bullet\text{DB18C6}$ ($M = \text{Li, Na, K, Rb, and Cs}$) complexes with the LIF spectrum of jet cooled DB18C6 reported by Kusaka et al. (Ref. 28).

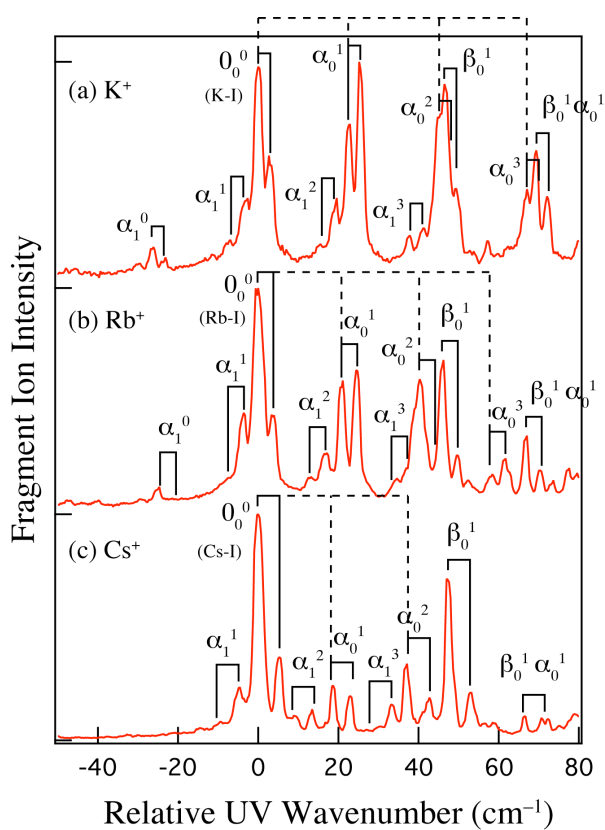


Figure 3. The UVPD spectra of the DB18C6 complexes with K^+ , Rb^+ , and Cs^+ around their respective origin bands. The horizontal axis is the UV wavenumber relative to the band origin. The doublet structure connected by solid lines is attributed to the exciton splitting due to the intramolecular interaction between the benzene rings. The low-frequency vibrations appearing in these spectra are labeled by α and β . Superscript and subscript integers with α and β denote quantum numbers of these vibrations in the S_1 and S_0 states, respectively. Progressions of vibrations α from the origin band are presented with dotted lines.

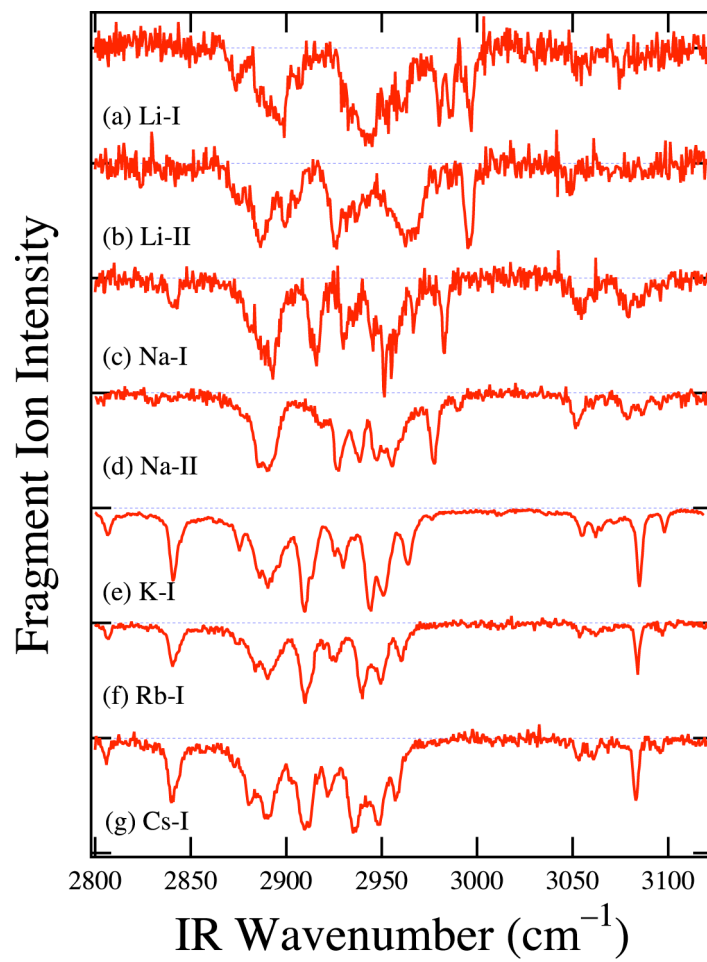


Figure 4. The IR-UV double-resonance spectra of the $M^+\bullet\text{DB18C6}$ ($M = \text{Li}, \text{Na}, \text{K}, \text{Rb}, \text{and Cs}$) complexes in the CH stretching region.

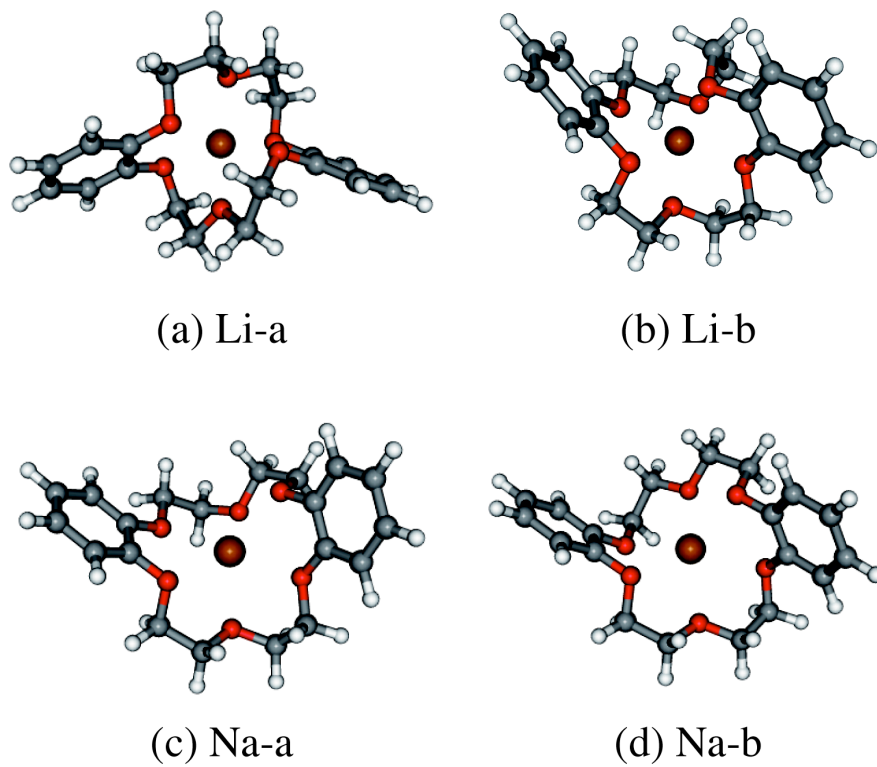
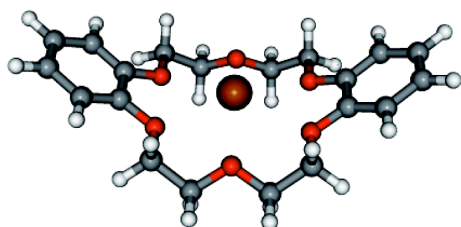
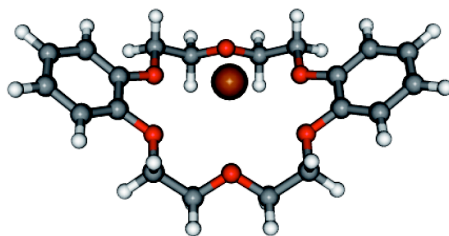


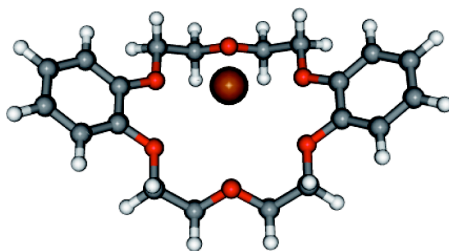
Figure 5. The structure of (a, b) $\text{Li}^+\cdot\text{DB18C6}$ and (c, d) $\text{Na}^+\cdot\text{DB18C6}$ complexes optimized at the M05-2X/6-31+G(d) level of theory.



(a) K-a (C_{2v})



(b) Rb-a (C_{2v})



(c) Cs-b (C_{2v})

Figure 6. The structure of (a) $K^+ \cdot DB18C6$, (b) $Rb^+ \cdot DB18C6$, and (c) $Cs^+ \cdot DB18C6$ complexes optimized at the M05-2X/6-31+G(d) level of theory.

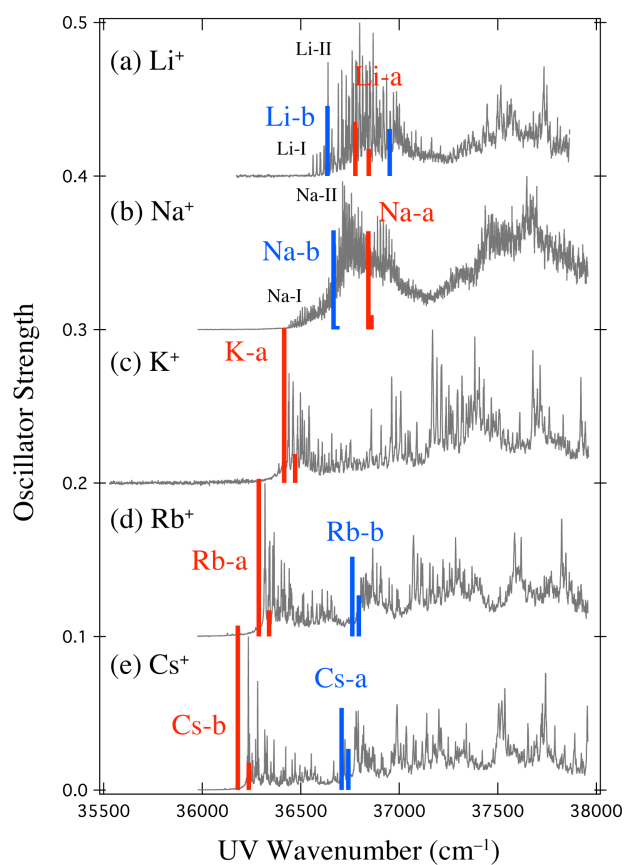


Figure 7. Oscillator strengths of electronic transitions for $M^+\bullet\text{DB18C6}$ ($M = \text{Li, Na, K, Rb, Cs}$) calculated with TD-DFT at the M05-2X/6-31+G(d) level and the Stuttgart RLC potential for Rb and Cs. Calculated transition energies are scaled with a scaling factor of 0.8340 in order to compare the calculated and experimental spectra. The scaling factor is determined so as to reproduce the transition energy of the origin band of $\text{K}^+\bullet\text{DB18C6}$.

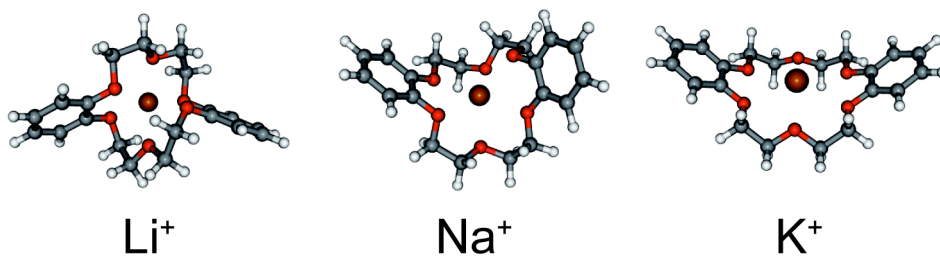
Table 1. Positions of the band origin (cm^{-1}), exciton splitting (cm^{-1}), and vibrational frequencies (cm^{-1}) observed in the UVPD spectra of the $\text{K}^+\cdot\text{DB18C6}$, $\text{Rb}^+\cdot\text{DB18C6}$, and $\text{Cs}^+\cdot\text{DB18C6}$ complexes.

	$\text{K}^+\cdot\text{DB18C6}$	$\text{Rb}^+\cdot\text{DB18C6}$	$\text{Cs}^+\cdot\text{DB18C6}$
Band Origin (cm^{-1})	36415	36319	36234
Exciton Splitting (cm^{-1})	2.7	4.0	5.3
mode α (S_0) (cm^{-1}) ^a	27	25	27
mode α (S_1) (cm^{-1}) ^a	23	21	19
mode β (cm^{-1}) ^a	47	46	47
mode 1 (cm^{-1})	754	754	754
mode 6 (cm^{-1})	546	547	547
mode 12 (cm^{-1})	968	967	967
mode A (cm^{-1}) ^a	903	903	905
mode B (cm^{-1}) ^a	1263	1267	1271

^a Unidentified normal modes are labeled with α , β , A, and B. Normal modes A and B are due to vibrations of the benzene rings.

Table 2. Distance between the center of the benzene rings and the difference in the distance between in the S_0 and S_1 states determined with geometry optimization at the M05-2X/6-31+G(d) level and Stuttgart RLC potential.

conformers	S_0 (Å)	S_1 (Å)	Difference (Å)
Li-a	7.87	7.94	0.07
Li-b	6.39	6.80	0.41
Na-a	7.48	7.98	0.50
Na-b	7.72	8.18	0.46
K-a	9.09	9.11	0.01
Rb-a	9.24	9.36	0.12
Cs-b	9.25	9.37	0.12



TOC Figure. Inokuchi et al.